

Record 1.1 V Open-Circuit Voltage for $\text{Cu}_2\text{ZnGeS}_4$ -Based Thin-Film Solar Cells Using Atomic Layer Deposition $\text{Zn}_{1-x}\text{Sn}_x\text{O}_y$ Buffer Layers

Nishant Saini,* Natalia M. Martin, Jes K. Larsen, Adam Hultqvist, Tobias Törndahl, and Charlotte Platzer-Björkman*

The $\text{Cu}_2\text{ZnGe}_x\text{Sn}_{1-x}\text{S}_4$ (CZGTS) thin-film solar cells have a limited open-circuit voltage (V_{OC}) due to bulk and interface recombination. Since the standard CdS buffer layer gives a significant cliff-like conduction band offset to CZGTS, alternative buffer layers are needed to reduce the interface recombination. This work compares the performance of wide bandgap $\text{Cu}_2\text{ZnGeS}_4$ (CZGS) solar cells fabricated with nontoxic $\text{Zn}_x\text{Sn}_{1-x}\text{O}_y$ (ZTO) buffer layers grown by atomic layer deposition under different conditions. The V_{OC} of the CZGS solar cell improved significantly to over 1 V by substituting CdS with ZTO. However, V_{OC} is relatively insensitive to ZTO bandgap variations. The short-circuit current is generally low but is improved with KCN etching of the CZGS absorber before deposition of the ZTO buffer layer. A possible explanation for the device behavior is the presence of an oxide interlayer for nonetched devices.

1. Introduction

The $\text{Cu}_2\text{ZnSnS}_4$ (CZTS) has received considerable interest as a promising solar cell material owing to its earth abundance and non-toxicity. The primary limitation of CZTS solar cells is their low open-circuit voltage (V_{OC}) due to bulk and interface recombination.^[1] The electronic properties of the CZTS absorber can be tuned by cationic substitution of isovalent Ge onto multivalent Sn sites to reduce Sn-related deep defects responsible for bulk recombination.^[2,3] $\text{Cu}_2\text{ZnGe}_x\text{Sn}_{1-x}\text{S}_4$ (CZGTS) absorbers show a high absorption coefficient of 10^4 cm^{-1} with a tunable bandgap between 1.5 and 2.1 eV,^[4–6] making them a possible

candidate for multijunction solar cells and band gap-graded devices.^[7–9]


We have previously reported the formation of a Ge-Sn gradient toward the rear interface of CZGTS absorbers made by sulfurizing a $\text{Cu}_2\text{ZnGeS}_4$ (CZGS) layer buried underneath a CZTS layer.^[10,11] Since the diffusion of Ge and Sn occurs faster through grain boundaries than grains,^[10,12] the accumulation of Ge on absorber interfaces easily occurs during sulfurization, which modifies the bandgap energy at the interfaces. The importance of the conduction band offset (CBO) at the absorber and buffer interface is well established.^[13] High efficiency $\text{Cu}(\text{In,Ga})\text{Se}_2$ solar cells often feature a close to flat conduction band align-

ment.^[14,15] A cliff-like band alignment ($\text{CBO} < 0$) may cause detrimental interface recombination, whereas a large spike ($\text{CBO} > 0.5 \text{ eV}$) blocks the photocurrent and decreases the fill factor.^[16] The CZTS/CdS interface is generally assumed to be cliff-like (-0.3 eV)^[17] (see Figure 1). The cliff-like band alignment is expected to increase with Ge incorporation due to upward shift in the conduction band minima (CBM) of CZGTS.^[18–20] This results in an increase in the CBO to $\approx -0.7 \text{ eV}$ ^[19] for the CZGS/CdS interface, which emphasizes the importance of replacing the CdS buffer layer.

The $\text{Zn}_x\text{Sn}_{1-x}\text{O}_y$ (ZTO) can be used as an alternative non-toxic substitute for the commonly used CdS buffer layer due to the possibility of band edge movement by either compositional change^[21] or deposition temperature,^[22] leading to reduced cliff-like alignment for CZGS absorbers (Figure 1). Moreover, the bandgap of CZGS^[10,23] is comparable to CdS,^[24] which results in significant parasitic absorption in the CdS. The wide bandgap ZTO^[22] can reduce the parasitic short wavelength absorption loss compared with the CdS^[24] buffer layer.

The CZGS can be a potential alternative to expensive wide bandgap GaP (2.3 eV)^[25,26] single junction solar cell. It can be suitable for use as a wide bandgap solar cell in tandem solar cell applications. In addition, alternative buffer layers have not been investigated for CZGS solar cell application to the best of our knowledge. As a result, the substitution of CdS with ZTO buffer layers on CZGS is investigated in this study. The deposition temperature of ZTO buffer layer is varied to observe

N. Saini, N. M. Martin, J. K. Larsen, A. Hultqvist, T. Törndahl, C. Platzer-Björkman
Division of Solar Cell Technology
Department of Materials Science and Engineering
Uppsala University
751 21 Uppsala, Sweden
E-mail: nishant.saini@angstrom.uu.se;
charlotte.platzer@angstrom.uu.se

 The ORCID identification number(s) for the author(s) of this article can be found under <https://doi.org/10.1002/solr.202100837>.

© 2021 The Authors. Solar RRL published by Wiley-VCH GmbH. This is an open access article under the terms of the Creative Commons Attribution License, which permits use, distribution and reproduction in any medium, provided the original work is properly cited.

DOI: 10.1002/solr.202100837

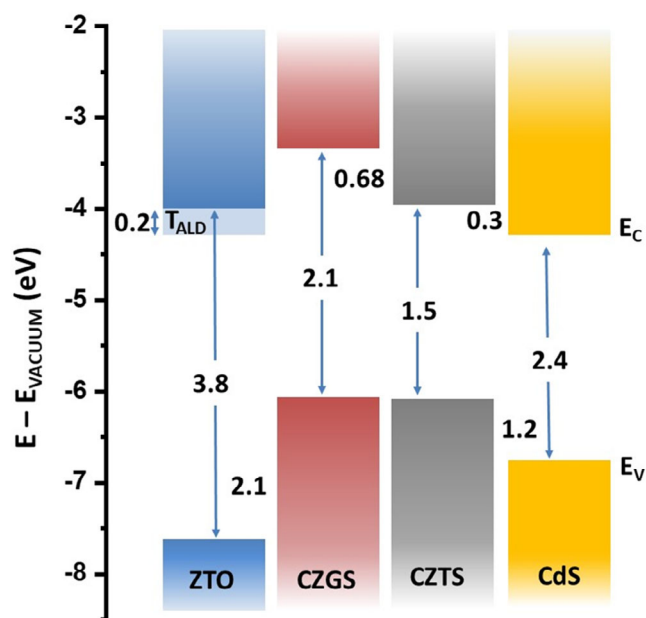


Figure 1. Approximate band offsets of ZTO, CdS, CZGS, and CZTS estimated from the literature.^[22,34,37,38] The band alignment of ZTO has been shown to change with ALD growth temperature (T_{ALD}) from 90 to 120 °C. Low temperature ZTO depositions were chosen to decrease the negative offset between CZGS and ZTO.

the effect on PV performance with varying ZTO bandgap energy.

2. Result and Discussion

2.1. CZGS Material Properties

The compositions of the different sputtered CZGS precursors are listed in **Table 1**, together with the sample naming of corresponding solar cell absorbers. The CZGS absorbers are prepared on TiN/Mo/SLG substrate. Coating of a thin TiN (≈ 20 nm) interlayer on Mo-coated (≈ 350 nm) glass improves the CZGS adhesion on the substrate (Mo/SLG)^[11] after the annealing of the precursors in the sulfur atmosphere. The grazing incidence X-

Table 1. The composition of CZGS precursors measured with XRF calibrated by RBS. The compositions of the reference precursors were measured on Mo/SLG substrate, and precursors on TiN-coated Mo/SLG were fabricated in the same batch. The average measurement error is indicated next to the heading for elemental ratios.

Batch	Composition		Sample naming
	Cu/Ge[± 0.05]	Zn/(Cu+Ge) [± 0.003]	
A	1.97	0.37	A1, A2, A3, A4, A5, A9, A10, A11, A12
B	2.02	0.38	B1, B2, B3
C	1.74	0.4	C
D	1.83	0.39	D

ray diffraction (GIXRD) pattern of the samples confirms the formation of crystalline CZGS (see **Figure 2a**). ZnS^[27] phases are detected; however, other secondary phases such as Cu_{2-x}S, Zn₂GeS₄,^[28] Cu₂GeS₃,^[29,30] and GeO₂ could be present but are not visible by X-ray diffraction due to peak overlap or small volume. The microstructural properties of the annealed CZGS absorbers are shown in Figure S1 in the supporting information (SI) (cross-sectional scanning electron microscopy [SEM]). These examples are representative of all batches A–D. After annealing, the typical absorber thickness is 750 nm, and the average CZGS grain size (≈ 200 nm) is similar in the cross-sectional SEM images of all the CZGS solar cells (Figure S1, Supporting Information).

The presence of CZGS was also verified by Raman spectroscopy of the samples with excitation of 532 nm laser (Figure S2, Supporting Information), which showed (359 cm^{-1}) A¹ and (295 cm^{-1}) A² vibrational modes of CZGS. The room temperature PL emission spectra (Figure S3, Supporting Information) of the samples showed a typical bandgap position of CZGS at 1.95 eV along with an unknown broad and intense peak at 1.4 eV. The samples were tilted to $\approx 45^\circ$, and PL spectra were remeasured in order to rule out that the 1.4 eV peak was caused by optical interference.^[31]

The CZGS films (Batch D) were also fabricated on SLG substrate for optical measurements. A Tauc's plot is shown in the Figure 2b, together with Raman spectra (Figure 2c) of the same film. An optical bandgap of 2.2 eV is determined from the Tauc's plot. The estimated optical bandgap from reflectance and transmittance spectroscopy of CZGS is higher than the PL bandgap of the CZGS. Such offset is well known in CZTS, where it is related to band tailing from high density of defects such as Cu-Zn antisites.^[32]

The influence of KCN etching on possible secondary phases at the absorber surface is of interest since both etched and non-etched absorbers were used in this study, as discussed below. In a separate X-ray photoelectron spectroscopy (XPS) study using CZTS and alloyed CZGS samples (Figure S4, Supporting Information), oxides present before KCN etching, most likely assigned to SnO_x for CZTS and GeO₂ for Ge containing CZGS, were removed after KCN etching.

2.2. ZTO Material Properties

The ZTO buffer layers were fabricated on top of the annealed CZGS films with SLG monitoring pieces for composition and thickness determination in each atomic layer deposition (ALD) run. As seen in **Table 2**, bandgap widening of ZTO is obtained at lower T_{ALD} , which can be an effect of lower film density or a quantum confinement effect from ZnO crystallites of decreasing size.^[22] The thickness of the ZTO layer is changed with a varying number of cycles at a fixed T_{ALD} . Figure S5, Supporting Information, illustrates the XPS of ZTO coatings, grown under various ALD deposition conditions, on CZGS absorbers. The spectra reveal mainly signals from the ZTO overlayer (Zn, Sn, and O). Some C contamination is observed at the surface of all samples, which is likely due to samples being exposed to air prior to XPS measurements. However, we cannot exclude that some C incorporation may also take place during the ALD

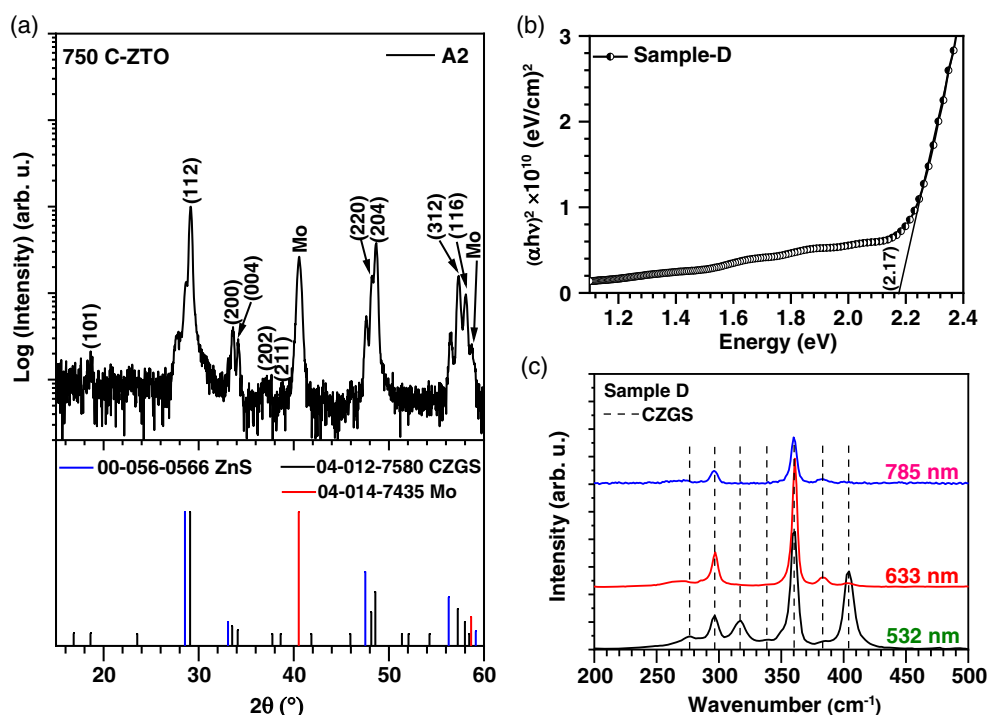


Figure 2. a) Grazing incidence X-ray diffraction pattern of a ZTO coated CZGS absorber fabricated on TiN/Mo/SLG. The XRD peak positions are consistent with the reference patterns of CZGS,^[39] Mo,^[40] and ZnS.^[27] b) Tauc's plot of CZGS indicates that the optical bandgap is around 2.2 eV. c) Raman spectra of CZGS under excitation wavelength of 532, 633, and 785 nm laser.

deposition. Further, no signals from the absorber (Cu, Ge, or S) were observed on any samples after ZTO deposition,

Table 2. The naming of precursors, as well as the deposition conditions and properties of ZTO deposited on soda-lime glass (SLG), are shown for each deposition. The composition of the ZTO is measured by XRF calibrated with RBS. The thickness of ZTO films is roughly estimated from XRF measurements. Bandgap values are taken from previous publications using the same deposition parameters and confirmed for the 90 °C sample in this study (Figure S6, Supporting Information).

Deposition temperature [°C]	Name	No. of ALD cycles [C]	Composition (Sn/(Sn+Zn)) on SLG	Thickness on SLG [nm]	Bandgap [eV]
90	A1	1000	0.19	26	3.7 ^{a)}
	A2	750	0.14	17	
100	A3	1000	0.23	33	3.6 ^[22]
	A4	750	0.21	23	
	A5	500	0.21	15	
	A6	1000	0.18	42	
110	A7	750	0.20	30	
	A8	500	0.24	17	
120	B1	1000	0.16	44	3.5 ^[22]
	B2	750	0.18	30	
	B3	500	0.16	18	

^{a)}From Tauc's plot in Figure S6, Supporting Information.

indicating that the buffer layers grown in this work are completely covering the CZGS absorbers due to the conformal^[33] growth of ZTO. The thicknesses of the various ZTO films on soda-lime glass are listed in Table 2. However, ZTO typically grows thinner^[22,34] on absorbers such as CZTS or CIGS than on SLG, and this can also be expected for CZGS. Due to the amorphous nature and small volume of ZTO interlayers, these could not be detected using XRD measurement of the ZTO coated CZGS.

2.3. CZGS Solar Cells with Different ZTO Deposition Conditions

In this section, the effect of various ZTO layer thicknesses grown at different ALD deposition temperatures ($T_{\text{ALD}} = 90$ to 120 °C) on the CZGS devices is investigated. Each batch of CZGS precursors was sulfurized separately for each ZTO deposition temperature. **Figure 3** (J - V and EQE in Figures S7–S10, Supporting Information) shows the solar cell parameters of CZGS solar cells with varying ZTO deposition conditions. **Table 3** summarizes the J - V parameters of the best CZGS solar cells with ZTO layers. Due to issues with partial or complete delamination of the CZGS during KCN etching, the samples in Table 3, and Figure 3 were made without etching, i.e., completely dry processing of the full device. As seen in Figure 3, the V_{OC} trend is relatively flat and shows some scatter, especially for 750 cycles. The highest V_{OC} of up to 1.1 V is achieved for T_{ALD} of 100 °C and 1000 cycles corresponding to a thickness of around 33 nm (on

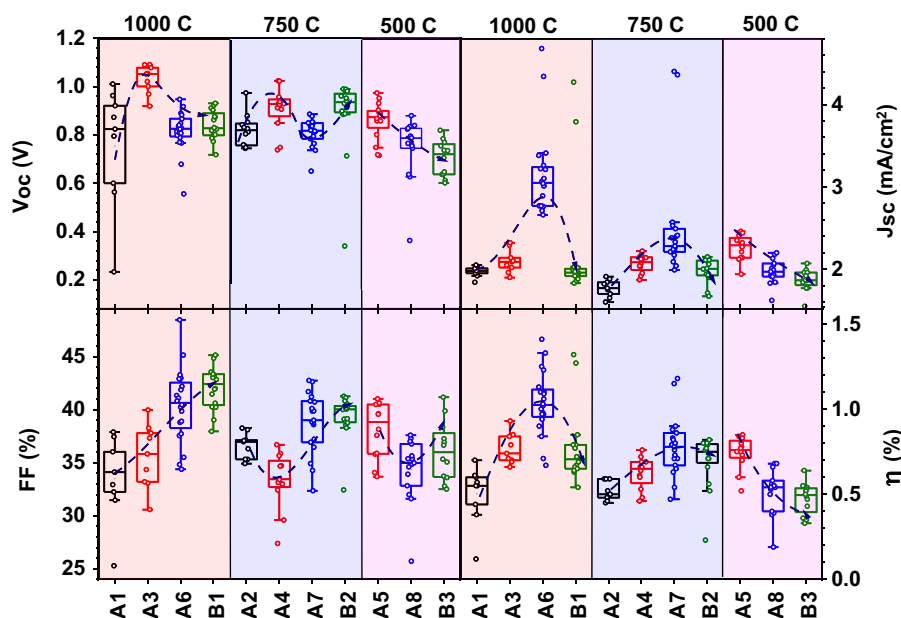


Figure 3. The solar cell parameters of a CZGS solar cell with ZTO buffer layers employing different ALD deposition conditions. The number of deposition cycles of ZTO are varied to optimize the thickness of the ZTO buffer layers. The device parameters are plotted in order of increasing deposition temperature from 90 to 120 °C within each group defined by the number of ALD cycles.

Table 3. Solar cell parameters of CZGS absorbers with different ZTO buffer layers. The EQE of sample B2 could not be obtained (see Figure S10, Supporting Information). The Voc deficit ($E_g/q-V_{oc}$) is based on the optical bandgap of 2.2 eV.

Sample name	Solar cell parameters					
	J_{sc} [mA cm^{-2}]	V_{oc} (V)	$E_g/q-V_{oc}$ [V]	FF [%]	η [%]	J_{sc} by EQE [mA cm^{-2}]
A1	2.0	0.963	1.237	36	0.69	2.1
A2	1.8	0.842	1.358	38	0.58	1.7
A3	2.1	1.078	1.122	38	0.86	2.5
A4	2.2	0.957	1.243	36	0.76	2.3
A5	2.4	0.974	1.226	36	0.85	2.5
A6	3.2	0.917	1.283	45	1.32	2.9
A7	2.2	0.854	1.346	43	0.81	2.3
A8	2.1	0.88	1.320	35	0.65	2.0
B1	2.0	0.931	1.269	45	0.84	2.2
B2	2.0	0.989	1.211	40	0.79	–
B3	1.9	0.819	1.381	40	0.62	1.8

SLG). V_{oc} of over 900 mV is seen for all T_{ALD} and thickest ZTO (1000 c), but the scatter for 90 °C is large. For 1000 and 750 cycles, the highest J_{sc} is seen at T_{ALD} 110 °C, but the most noticeable result is the much higher J_{sc} of some devices at 110 and 120 °C. The fill factor (FF) shows some trend of increasing with decreasing T_{ALD} for the thickest ZTO layers. Efficiencies are around 0.5%–1% with the highest values of up to 1.5% with outlier devices at 110 °C having much higher J_{sc} . For further improvement of CZGS/ZTO devices, the strongly suppressed J_{sc} needs to be increased in order to not counteract the improved V_{oc} . The high J_{sc} outlier samples indicate that some uncontrolled blocking of the current can occur. Also, the limited

influence on V_{oc} from changes in ZTO bandgap energy, and expected accompanied change in CBM position, should be noted. This indicates that the CZGS/ZTO interface is not changed as expected in this series.

2.4. Effect of CZGS Absorber Etching on Solar Cell Performance

Some samples could be fabricated including a KCN etch prior to buffer layer deposition without absorber delamination, which are described here. ZTO layers were deposited at 90 °C and 1599 cycles on etched CZGS absorbers and compared with non-etched

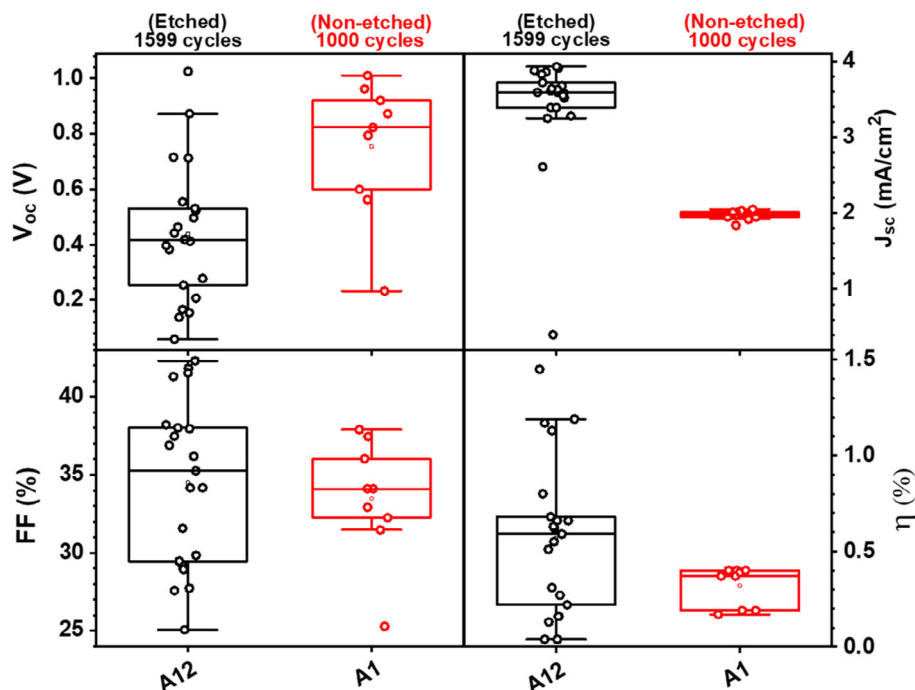


Figure 4. Solar cell parameters of devices fabricated on etched and non-etched CZGS absorber.

samples with 1000 cycles. CZGS precursors sputter deposited and sulfurized in the same batch were used in this study. To make comparisons using absorbers from the same batch is expected to be more important than comparing identical ZTO thicknesses. Raman and PL spectra of ZTO coated non-etched and etched CZGS absorber both showed typical CZGS vibrational modes with excitation of 532 nm laser (shown in the Figure S11, Supporting Information). **Figure 4** shows the photovoltaic performance

parameters of solar cells with ZTO, with and without KCN etching (JV curves are shown in Figure S12, Supporting Information). The mean V_{OC} is decreased with etching, but the clear difference is in the short-circuit current that is strongly increased with etching to around twice the value. KCN etching is expected to be useful to remove secondary phases on the front surface, such as GeO_2 (Figure S4, Supporting Information) or Cu_xS .^[35] It is possible that the higher current after etching and high J_{SC} for the non-etched

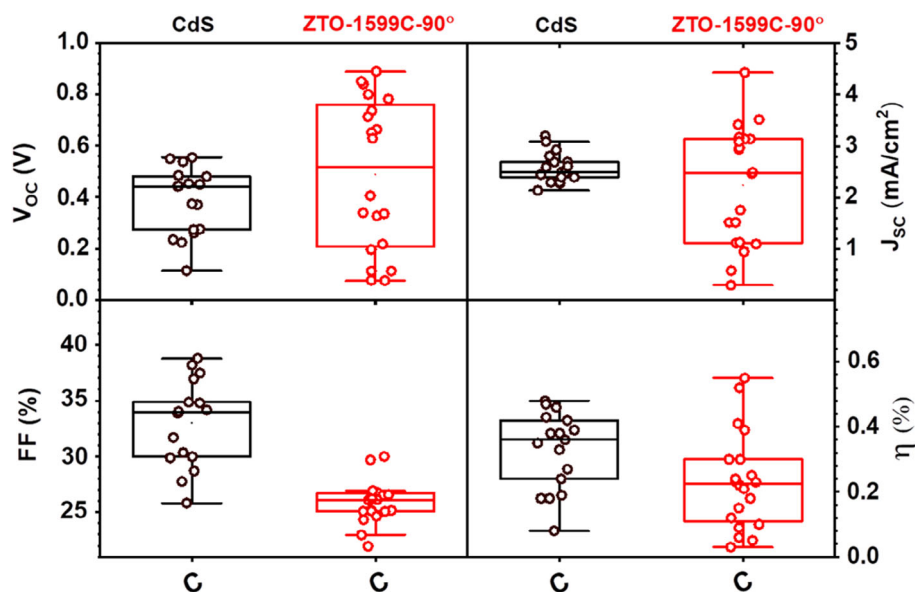


Figure 5. Solar cell device performance of CZGS absorber with different buffer layers. CZGS absorbers were etched prior to deposition of any buffer layers and ZTO layers were deposited at 90 °C for 1599 cycles.

samples at T_{ALD} 110 and 120 °C have similar explanation, such as absence of blocking phases at the interface. GeO_2 has larger bandgap energy than SnO_2 , and since the removal of GeO_2 in KCN is supported by XPS investigations (Figure S4, Supporting Information), this is a likely explanation. This would also explain the results in Section 2.2, where ZTO deposition temperature did not clearly influence V_{OC} as expected. A dielectric interlayer between CZGS and ZTO could dominate the interface properties and device behavior. Such an interlayer could also reduce recombination at the interface and this could explain the reduced V_{OC} with etching. However, further studies are required to more clearly identify such an interlayer to understand the influence of etching on CZGS and the strongly varying J_{SC} .

2.5. Buffer layer comparison on CZGS absorber

Figure 5 shows the performance comparison of CZGS solar cells with CdS and ZTO buffer layers grown at an ALD deposition temperature of 90 °C for 1599 cycles. In both cases, KCN etching was employed. Due to issues with partial or complete delamination during the KCN etching process, as also reported previously,^[11] only a few devices with CdS buffer layer could be made. This is also the most likely reason for the wide spread in device performance over the samples. The FF is reduced with ZTO buffer compared with CdS buffer on these CZGS absorbers, however, Figure 4 shows higher FF for etched CZGS/ZTO devices. The J_{SC} varies between samples, but is higher when replacing the CdS layer with ZTO buffer layer on etched CZGS absorbers. The average V_{OC} is marginally increased when the ZTO buffer layer is used, but the peak V_{OC} is higher for ZTO; however, the overall device performance remains similar.

As compared with CdS, the ZTO bandgap is larger with a higher CBM level for low deposition temperature, as shown in Figure 1.^[21,34] Ericson et al.^[34] showed that an optimized band alignment (small spike-like) can yield higher V_{OC} with ZTO buffer layer on CZTS due to reduced interface recombination.^[16,34] The band alignment between CZGS and high bandgap ZTO, on the other hand, most likely remains cliff-like in this study. Still, significant V_{OC} improvement is seen, but further increase in CBM could possibly give additional improvements. In addition to the interface recombination, the device properties are affected by bulk recombination and possibly current-reducing secondary phases such as GeO_2 and ZnS .

3. Conclusion

$\text{Cu}_2\text{ZnGeS}_4$ absorbers with a wide optical bandgap (2.2 eV) were used to make thin-film solar cells with different buffer layers. A V_{OC} greater than 900 mV was measured on best devices after substituting CdS with ZTO deposited on KCN etched CZGS, compared with below 600 mV for CdS. A record V_{OC} of 1.1 V of non-etched CZGS absorbers was obtained for devices with an ALD temperature of 100 °C, but the V_{OC} was relatively constant for all ZTO deposition temperatures, contrary to expectations. The J_{SC} of CZGS solar cell increased with etching of the absorber prior to deposition of the ZTO buffer layer, which could likely be attributed to the removal of oxide phases. Such an oxide interlayer could also be the explanation for the small

variation in device performance with ZTO deposition temperature. ZTO appears compatible with CZGS and further studies on lower bandgap CZGTS, for which a suitable CBO to ZTO is expected, would be interesting. For large bandgap CZGS, further studies of surface etching combined with another buffer layer with even higher CBM is recommended.

4. Experimental Section

CZGS Fabrication: In this study, clean 1 mm soda-lime glass (SLG) was coated with 350 nm Mo by DC (direct current) sputtering in 0.8 Pa Ar atmosphere. An adhesive TiN interlayer was reactively sputter deposited on the Mo-coated SLG (Von Ardenne sputter system) at deposition pressure 0.8 Pa of Ar:N_2 mixture in the ratio of 20:45 sccm. The sputtering (Kurt J. Lesker sputter system) of 7.62 cm diameter CuS (DC, 1.4 W cm^{-2}), Ge (DC, 0.59 W cm^{-2}), and ZnS (radio frequency [RF], 3.51 W cm^{-2}) targets was used to deposit CZGS layers onto TiN/Mo/SLG substrates in 0.7 Pa Ar atmosphere. The base pressure of each of the sputter systems was below 3×10^{-5} Pa. CZGS precursor composition was measured by XRF, calibrated by RBS (Table 1). The temperature of the substrate holder was maintained at 250 °C with a rotation of 0.33 Hz during sputter-deposition. CZGS precursors were air exposed while transferring them to vacuum storage or tube furnace.

The precursors were sulfurized just before deposition of the buffer layers. CZGS precursors were loaded in a pyrolytic-coated graphite box (GB) with a hole of 3 mm diameter in the lid to allow air removal. GB containing 110 mg sulfur was introduced into a preheated tube furnace and sulfurized under stable pressure of 47 kPa Ar. The temperature of the substrate holder increased up to 581 °C over a 13 min. dwell time. Additional information about the baseline annealing is available in the following reference.^[11]

During initial trials, CZGS absorbers were potassium cyanide (KCN) etched to remove secondary and water-soluble phases, leading to partial or complete delamination, despite using adhesive TiN interlayer. As a result, only a few CZGS solar cells were fabricated with ZTO and CdS buffer layers after KCN etching. However, due to the partial or complete delamination of CZGS, no etching was done in the main ZTO buffer deposition series. The temperature and thickness of the ZTO layers were varied to investigate their impact on the solar cell performance.

ZTO Growth: The $\text{Zn}_x\text{Sn}_{1-x}\text{O}_y$ films were deposited using thermal ALD at temperatures of 90, 100, 110, and 120 °C in a Microchemistry F120 viscous flow reactor using N_2 carrier gas (99.9999%). The Zn precursor $\text{Zn}(\text{C}_2\text{H}_5)_2$ (diethyl-zinc, DEZ, and AkzoNobel TCO grade) was effused into the reactor. The Sn precursor $\text{Sn}(\text{N}(\text{CH}_3)_2)_4$ (tetraakisdimethylamino-tin, TDMASn, SAFC research grade) was heated to 40 °C to achieve enough vapor pressure by sublimation to effuse into the reactor. Finally, the O precursor H_2O (deionized water, 18 M Ω cm) was effused into the chamber. To create the ternary ZTO compound, subcycles of SnO_x and ZnO were alternated in a 1 to 1 ratio. The SnO_x subcycle was TDMASn/purge/ H_2O /purge using pulse times of 0.4/0.8/0.4/0.8 s respectively, while the ZnO subcycle was DEZn/purge/ H_2O /purge using pulse times of 0.4/0.8/0.4/0.8 s respectively. These pulse times leads to reaction dynamics that reaches saturation or close to saturation at the deposition temperatures of 90, 100, 110, and 120 °C.

The ALD reactor was conditioned with Zn and Sn precursors after stabilization at the required temperature. ZTO buffer layers were deposited on CZGS absorbers while keeping the same dosage of Zn and Sn precursors inside the ALD reactor; however, the composition of the prepared ZTO could be affected by the reaction temperature. In the ZTO series, the thickness was varied by using between 500 and 1599 cycles, as well as deposition temperature between 90 °C and 120 °C. At 90 °C, CZGS solar cells with 500 c ZTO could not be prepared due to a faulty composition of ZTO layer in the ALD batch. ALD deposition was not reproduced due to shortage of CZGS samples from the same sputter run.

The fabrication of devices was completed by sequential sputter deposition of 80 nm i-ZnO and 170 nm Al:ZnO on the buffer coated absorbers. The samples were mechanically scribed into 0.05 cm² solar cells.^[11,36]

The JV measurements were performed in dark and illuminated conditions using a Newport ABA solar simulator, and the external quantum efficiency (EQE) was determined using a homebuilt setup. The light intensity in the J–V setup was calibrated to match the calculated current density of the CZGS solar cell in the EQE setup.

The phase crystallinity and purity of the sample were determined using X-ray diffraction with the aid of GIXRD (grazing incidence X-ray diffraction). Cu K α 1 radiation (1.54056 Å) was used with a grazing incidence angle of 1.0° to measure the X-ray diffraction pattern of ZTO coated CZGS (XRD, Siemens D5000) in parallel beam geometry. Raman and photoluminescence (Renishaw inVia confocal Raman microscope equipped with an InGaAs and Si CCD detector) spectra of the ZTO-coated absorber were measured at room temperature under excitation of a 532 nm laser.

The X-ray photoelectron (Quantum 2000 ESCA microscope, Physical Electronics) spectra of the ZTO coated absorbers were measured using monochromatic Al K α radiation (1486.7 eV) and the measured spot size was 200 μ m. The samples were air exposed while transferring into the UHV system. The metallic composition of absorber films was determined using X-ray fluorescence (XRF, PANalytical Epsilon 5) calibrated with Ruthenium backscattering spectroscopy (RBS). Cross-section images were captured using a scanning electron microscope (SEM, Zeiss Leo 1530) equipped with an in-lens detector. The cross-section morphology was observed with a low-energy beam incident on the sample (5 kV, 175 nA beam current, and 30 μ m aperture size).

Supporting Information

Supporting Information is available from the Wiley Online Library or from the author.

Acknowledgements

The authors acknowledge funding from the Swedish Research Council (grant 2019-04793) and from the Swedish Foundation for Strategic Research (grant RMA15-0030).

Conflict of Interest

The authors declare no conflict of interest.

Data Availability Statement

The data that support the findings of this study are available from the corresponding authors upon reasonable request.

Keywords

band alignment, CZGS, KCN etching, solar cells, wide bandgap, ZTO

Received: October 11, 2021

Revised: November 26, 2021

Published online:

- [1] A. Walsh, S. Chen, S.-H. Wei, X.-G. Gong, *Adv. Mater.* **2012**, 2, 400.
- [2] S. Chen, A. Walsh, Y. Luo, J.-H. Yang, X. G. Gong, S.-H. Wei, *Phys. Rev. B* **2010**, 82, 195203.
- [3] S. Kim, J.-S. Park, A. Walsh, *ACS Energy Lett.* **2018**, 3, 496.

- [4] H. Matsushita, T. Ichikawa, A. Katsui, *J. Mater. Sci.* **2005**, 40, 2003.
- [5] S. Levchenko, D. Dumcenco, Y. S. Huang, K. K. Tiong, C. H. Du, *Opt. Mater.* **2011**, 34, 183.
- [6] I. Tsuji, Y. Shimodaira, H. Kato, H. Kobayashi, A. Kudo, *Chem. Mater.* **2010**, 22, 1402.
- [7] G. M. Ford, Q. Guo, R. Agrawal, H. W. Hillhouse, *Chem. Mater.* **2011**, 23, 2626.
- [8] Q. Guo, G. M. Ford, W.-C. Yang, B. C. Walker, E. A. Stach, H. W. Hillhouse, R. Agrawal, *J. Am. Chem. Soc.* **2010**, 132, 17384.
- [9] M. Jiang, Y. Li, R. Dhakal, P. S. Thapaliya, M. A. Mastro, J. Caldwell, F. J. Kub, X. Yan, *JPE* **2011**, 1, 019501.
- [10] N. Saini, J. K. Larsen, K. V. Sopiha, J. Keller, N. Ross, C. Platzer-Björkman, *Phys. Status Solidi* **2019**, 216, 1900492.
- [11] N. Saini, J. K. Larsen, K. Lindgren, A. Fazi, C. Platzer-Björkman, *J. Alloys Compd.* **2021**, 880, 160478.
- [12] A. D. L. Claire, *Lond. Edinb. Dublin Philos. Mag. J. Sci.* **1951**, 42, 468.
- [13] M. Gloeckler, J. R. Sites, *J. Phys. Chem. Solids* **2005**, 66, 1891.
- [14] D. Hauschild, D. Kreikemeyer-Lorenzo, P. Jackson, T. M. Friedlmeier, D. Hariskos, F. Reinert, M. Powalla, C. Heske, L. Weinhardt, *ACS Energy Lett.* **2017**, 2, 2383.
- [15] M. Morkel, L. Weinhardt, B. Lohmüller, C. Heske, E. Umbach, W. Riedl, S. Zweigart, F. Karg, *Appl. Phys. Lett.* **2001**, 79, 4482.
- [16] T. Minemoto, T. Matsui, H. Takakura, Y. Hamakawa, T. Negami, Y. Hashimoto, T. Uenoyama, M. Kitagawa, *Sol. Energy Mater. Sol. Cells* **2001**, 67, 83.
- [17] A. Santoni, F. Biccari, C. Malerba, M. Valentini, R. Chierchia, A. Mittiga, *J. Phys. D: Appl. Phys.* **2013**, 46, 175101.
- [18] A. S. R. Chesman, J. van Embden, E. Della Gaspera, N. W. Duffy, N. A. S. Webster, J. J. Jasieniak, *Chem. Mater.* **2014**, 26, 5482.
- [19] K. Tsuji, T. Maeda, T. Wada, *Jpn. J. Appl. Phys.* **2018**, 57, 08RC21.
- [20] Q. Shu, J.-H. Yang, S. Chen, B. Huang, H. Xiang, X.-G. Gong, S.-H. Wei, *Phys. Rev. B* **2013**, 87, 115208.
- [21] M. Kapilashrami, C. X. Kronawitter, T. Törndahl, J. Lindahl, A. Hultqvist, W.-C. Wang, C.-L. Chang, S. S. Mao, J. Guo, *Phys. Chem. Chem. Phys.* **2012**, 14, 10154.
- [22] J. Lindahl, J. Keller, O. Donzel-Gargand, P. Szaniawski, M. Edoff, T. Törndahl, *Sol. Energy Mater. Sol. Cells* **2016**, 144, 684.
- [23] D. Chen, N. M. Ravindra, *J. Alloys Compd.* **2013**, 579, 468.
- [24] M. R. Squillante, K. S. Shah, *Semiconductors and Semimetals* (Eds: T. E. Schlesinger, R. B. James), Elsevier, Amsterdam **1995**, pp. 465–491.
- [25] P. Suman, Sharma, P. Goyal, *Mater. Today: Proc.* **2020**, 28, 1593.
- [26] X. Lu, S. Huang, M. B. Diaz, N. Kotulak, R. Hao, R. Opila, A. Barnett, *IEEE J. Photovoltaics* **2012**, 2, 214.
- [27] H. E. Swanson, *Standard X-Ray Diffraction Powder Patterns*, Vol. II, U. S. Department of Commerce, National Bureau of Standards, Washington DC **1953**.
- [28] H. Haeuseler, H. J. Stork, *Mater. Res. Bull.* **1992**, 27, 925.
- [29] X. Jin, L. Zhang, G. Jiang, W. Liu, C. Zhu, *Sol. Energy Mater. Sol. Cells* **2017**, 160, 319.
- [30] M. Khanafer, O. Gorochov, J. Rivet, *Mater. Res. Bull.* **1974**, 9, 1543.
- [31] J. K. Larsen, S.-Y. Li, J. J. S. Scragg, Y. Ren, C. Häggglund, M. D. Heinemann, S. Kretzschmar, T. Unold, C. Platzer-Björkman, *J. Appl. Phys.* **2015**, 118, 035307.
- [32] T. Gokmen, O. Gunawan, T. K. Todorov, D. B. Mitzi, *Appl. Phys. Lett.* **2013**, 103, 103506.
- [33] J. Lindahl, J. T. Wätjen, A. Hultqvist, T. Ericson, M. Edoff, T. Törndahl, *Prog. Photovoltaics Res. Appl.* **2013**, 21, 1588.

- [34] T. Ericson, F. Larsson, T. Törndahl, C. Frisk, J. Larsen, V. Kosyak, C. Hägglund, S. Li, C. Platzer-Björkman, *Solar RRL* **2017**, 1, 1700001.
- [35] B.-A. Schubert, B. Marsen, S. Cinque, T. Unold, R. Klenk, S. Schorr, H.-W. Schock, *Prog. Photovoltaics Res. Appl.* **2011**, 19, 93.
- [36] J. K. Larsen, F. Larsson, T. Törndahl, N. Saini, L. Riekehr, Y. Ren, A. Biswal, D. Hauschild, L. Weinhardt, C. Heske, C. Platzer-Björkman, *Adv. Mater.* **2019**, 9, 1900439.
- [37] F. Larsson, N. S. Nilsson, J. Keller, C. Frisk, V. Kosyak, M. Edoff, T. Törndahl, *Prog. Photovoltaics Res. Appl.* **2017**, 25, 755.
- [38] T. Ericson, J. J. Scragg, A. Hultqvist, J. T. Wätjen, P. Szaniawski, T. Törndahl, C. Platzer-Björkman, *IEEE J. Photovoltaics* **2014**, 4, 465.
- [39] O. V. Parasyuk, L. V. Piskach, Y. E. Romanyuk, I. D. Oleksyuk, V. I. Zaremba, V. I. Pekhnyo, *J. Alloys Compd.* **2005**, 397, 85.
- [40] C. Bernuy-Lopez, M. Allix, C. A. Bridges, J. B. Claridge, M. J. Rosseinsky, *Chem. Mater.* **2007**, 19, 1035.